Geophysical Journal International

Geophys. J. Int. (2013) **193,** 960–969 doi: 10.1093/gji/ggt017

Lowrank finite-differences and lowrank Fourier finite-differences for seismic wave extrapolation in the acoustic approximation

Xiaolei Song,[1] Sergey Fomel[1] and Lexing Ying[2]

[1]*Bureau of Economic Geology, John A. and Katherine G. Jackson School of Geosciences, The University of Texas at Austin, University Station, Box X, Austin, TX* 78713-8972, *USA. E-mail: songxl@utexas.edu*

[2]*Department of Mathematics, The University of Texas at Austin,* 1 *University Station, Austin, TX* 78712, *USA.*

Accepted 2013 January 16. Received 2013 January 16; in original form 2012 February 6

SUMMARY

We introduce a novel finite-difference (FD) approach for seismic wave extrapolation in time. We derive the coefficients of the finite-difference operator from a lowrank approximation of the space-wavenumber, wave-propagator matrix. Applying the technique of lowrank finite-differences, we also improve the finite difference scheme of the two-way Fourier finite differences (FFD). We call the new operator lowrank Fourier finite differences (LFFD). Both the lowrank FD and lowrank FFD methods can be applied to enhance accuracy in seismic imaging by reverse-time migration. Numerical examples confirm the validity of the proposed technique.

Key words: Numerical solutions; Body waves; Seismic anisotropy; Computational seismology; Wave propagation; Acoustic properties.

1 INTRODUCTION

Wave extrapolation in time is crucial in seismic modelling, imaging (reverse-time migration) and full-waveform inversion. The most popular and straightforward way to implement wave extrapolation in time is the method of explicit finite differences (FDs), which is only conditionally stable and suffers from numerical dispersion (Wu *et al.* 1996; Finkelstein & Kastner 2007). In practice, a second-order FD for temporal derivatives and a high-order FD for spatial derivatives are often employed to reduce dispersion and improve accuracy. FD coefficients are conventionally determined using a Taylor-series expansion around zero wavenumber (Dablain 1986; Kindelan *et al.* 1990). Therefore, traditional FD methods are accurate primarily for long-wavelength components.

More advanced methods have been applied previously to FD schemes in the case of one-way wave extrapolation (downward continuation). Holberg (1987, 1988) designed the derivative operator by matching the spectral response in the wavenumber domain. Soubaras (1996) adopted the Remez exchange algorithm to obtain the L_∞-norm-optimized coefficients for second-derivative filters. Mousa *et al.* (2009) designed stable explicit depth extrapolators using projections onto convex sets (POCS). These approaches have advantages over conventional FD methods in their ability to propagate shorter-wavelength seismic waves correctly. To satisfy the general criterion for optimal accuracy (Geller & Takeuchi 1995), Geller & Takeuchi (1998) derived an optimally accurate time-domain finite difference method for computing synthetic seismograms for 1-D problems extended later to 2-D and 3-D (Takeuchi & Geller 2000). Liu & Sen (2009) proposed FD schemes for two-way scalar waves on the basis of time-space dispersion relations and plane-wave theory. Later on, they suggested adaptive variable-length spatial operators in order to decrease computing costs significantly without reducing accuracy (Liu & Sen 2011). The Liu-Sen scheme satisfies the exact dispersion relation and has greater accuracy and better stability than a conventional one. However, it still uses an expansion around the zero wavenumber.

In sedimentary rocks, anisotropic phenomena are often observed as a result of layering lithification, which is described as transversely isotropic (TI). Tectonic movement of the crust may rotate the rocks and tilt the natural vertical orientation of the symmetry axis (VTI), causing a tilted TI (TTI) anisotropy. Wavefields in anisotropic media are well described by the anisotropic elastic-wave equation. However, in practice, seismologists often have little information about shear waves and prefer to deal with scalar wavefields. Conventional *P*-wave modelling may contain shear wave numerical artefacts in the simulated wavefield (Grechka *et al.* 2004; Duveneck *et al.* 2008; Zhang *et al.* 2009). Those artefacts as well as sharp changes in symmetry-axis tilting may introduce severe numerical dispersion and instability in modelling. Yoon *et al.* (2010) proposed to reduce the instability by introducing elliptical anisotropy in regions with rapid tilt changes. Fletcher *et al.* (2009) suggested to include a finite *S*-wave velocity to enhance stability when solving coupled equations. These methods can alleviate the instability problem; however, they may alter the wave propagation kinematics or leave residual *S*-wave components in the *P*-wave simulation. A number of spectral methods are proposed to provide solutions which can completely avoid the shear wave artefacts (Etgen & Brandsberg-Dahl 2009; Chu & Stoffa 2011; Song & Fomel 2011; Fomel *et al.* 2012; Fowler & Lapilli 2012; Cheng & Kang 2012; Zhan *et al.* 2012) at the cost of several Fourier transforms per time step. These methods

differ from conventional pseudo-spectral methods (Gazdag 1981; Fornberg 2002), because they approximate the space-wavenumber mixed-domain propagation matrix instead of a Laplacian operator.

Our goal is to design an FD scheme that matches the spectral response in the mixed space-wavenumber domain for a wide range of spatial wavenumbers. The scheme is derived from the lowrank approximation of the mixed-domain operator (Fomel *et al.* 2010, 2012) and its representation by FD with adapted coefficients. We derive this kind of FD schemes which we call lowrank FD or LFD for both isotropic and TTI media. Using this approach, we only need to compute the FD coefficients once and save them for the whole process of wave extrapolation or reverse-time migration. The method is flexible enough to control accuracy by the rank of approximation and by FD order selection.

The paper is organized as follows. We first give a brief review of the lowrank approximation method. As a spectral method, it provides an accurate wave extrapolation, but it is not optimally efficient. Next, we present the derivation of LFD. LFD as an FD method can reduce the cost and is also more adaptable for parallel computing on distributed computer systems. We also propose lowrank Fourier FD (LFFD), by replacing the original FD operator in the two-way Fourier FD (FFD) (Song & Fomel 2011) with the corresponding LFD. LFFD improves the accuracy of FFD, in particular in TTI media. A number of synthetic examples of increasing complexity validate the proposed methods. In this paper, we solve the acoustic wave equation in constant-density media, aiming at incorporating wave extrapolation with LFD and LFFD into seismic imaging by reverse-time migration. It is possible to extend LFD and LFFD to variable-density media by factoring the second-order k-space operator into first-order parts (Tabei *et al.* 2002; Song *et al.* 2012).

2 THEORY

2.1 Lowrank approximation

The following acoustic-wave equation is widely used in seismic modelling and reverse-time migration (Etgen *et al.* 2009)

$$\frac{\partial^2 p}{\partial t^2} = v(\mathbf{x})^2 \nabla^2 p \ , \tag{1}$$

where $\mathbf{x} = (x_1, x_2, x_3)$, $p(\mathbf{x}, t)$ is the seismic pressure wavefield and $v(\mathbf{x})$ is the propagation velocity. Assuming a constant velocity, v, after Fourier transform in space, we could obtain the following explicit expression,

$$\frac{d^2 \hat{p}}{dt^2} = -v^2 |\mathbf{k}|^2 \hat{p} \ , \tag{2}$$

where

$$\hat{p}(\mathbf{k}, t) = \int_{-\infty}^{+\infty} p(\mathbf{x}, t) e^{i\mathbf{k}\cdot\mathbf{x}} \mathrm{d}\mathbf{x} \ , \tag{3}$$

and $\mathbf{k} = (k_1, k_2, k_3)$.

Eq. (2) has an explicit solution:

$$\hat{p}(\mathbf{k}, t + \Delta t) = e^{\pm i |\mathbf{k}| v \Delta t} \hat{p}(\mathbf{k}, t) \ . \tag{4}$$

A second-order time-marching scheme and the inverse Fourier transform lead to the well-known expression (Etgen 1989; Soubaras & Zhang 2008):

$$p(\mathbf{x}, t+\Delta t) + p(\mathbf{x}, t-\Delta t) = 2 \int_{-\infty}^{+\infty} \hat{p}(\mathbf{k}, t) \cos(|\mathbf{k}| v \Delta t) e^{-i\mathbf{k}\cdot\mathbf{x}} d\mathbf{k}. \tag{5}$$

Eq. (5) provides an efficient solution in the case of a constant-velocity medium with the aid of the fast Fourier transform (FFT). When velocity varies in space, eq. (5) can provide an approximation by replacing v with $v(\mathbf{x})$. In such a case, a mixed-domain term, $\cos(|\mathbf{k}| v(x) \Delta t)$, appears in the expression. As a result, the computational cost of a straightforward application of eq. (5) is $O(N_x^2)$, where N_x is the total size of the 3-D space grid.

Fomel *et al.* (2010, 2012) showed that the mixed-domain matrix,

$$W(\mathbf{x}, \mathbf{k}) = \cos(|\mathbf{k}| v \Delta t), \tag{6}$$

can be efficiently decomposed into a separate representation of the following form:

$$W(\mathbf{x}, \mathbf{k}) \approx \sum_{m=1}^{M} \sum_{n=1}^{N} W(\mathbf{x}, \mathbf{k}_m) a_{mn} W(\mathbf{x}_n, \mathbf{k}), \tag{7}$$

where $W(\mathbf{x}, \mathbf{k}_m)$ is a submatrix of $W(\mathbf{x}, \mathbf{k})$ that consists of selected columns associated with $\mathbf{k}_\mathrm{m}$, $W(\mathbf{x}_n, \mathbf{k})$ is another submatrix that contains selected rows associated with $\mathbf{x}_\mathrm{n}$, and a_{mn} stands for the middle matrix coefficients. The construction of the separated form (7) follows the method of Engquist & Ying (2009). The main observation is that the columns of $W(\mathbf{x}, \mathbf{k}_m)$ need to span the column space of the original matrix and that the rows of $W(\mathbf{x}_n, \mathbf{k})$ need to span the row space as well as possible.

Representation (7) speeds up the computation of $p(\mathbf{x}, t + \Delta t)$ because

$$p(\mathbf{x}, t + \Delta t) + p(\mathbf{x}, t - \Delta t) = 2 \int e^{-i\mathbf{x}\mathbf{k}} W(\mathbf{x}, \mathbf{k}) \hat{p}(\mathbf{k}, t) d\mathbf{k}$$

$$\approx 2 \sum_{m=1}^{M} W(\mathbf{x}, \mathbf{k}_m) \left(\sum_{n=1}^{N} a_{mn} \left(\int e^{-i\mathbf{x}\mathbf{k}} W(\mathbf{x}_n, \mathbf{k}) \hat{p}(\mathbf{k}, t) d\mathbf{k} \right) \right). \tag{8}$$

Evaluation of eq. (8) requires N inverse FFTs. Correspondingly, the lowrank approximation reduces the cost to $O(NN_x \log N_x)$, where N is a small integer, which is related to the rank of the above decomposition and can be automatically calculated at some given error level with a pre-determined Δt. Increasing the time step size Δt may increase the rank of the approximation (M and N) and correspondingly the number of the required Fourier transforms.

As a spectral method, the lowrank approximation is highly accurate. However, its cost is several FFTs per time step. Our goal is to reduce the cost further by deriving an FD scheme that matches the spectral response of the output from the lowrank decomposition.

2.2 Lowrank finite differences

In a matrix notation, the lowrank decomposition problem takes the following form:

$$\mathbf{W} \approx \mathbf{W}_1 \cdot \mathbf{A} \cdot \mathbf{W}_2, \tag{9}$$

where $\mathbf{W}$ is the $N_x \times N_x$ matrix with entries $W(\mathbf{x}, \mathbf{k})$, $\mathbf{W}_1$ is the submatrix of $\mathbf{W}$ that consists of the columns associated with $\{\mathbf{k}_m\}$, $\mathbf{W}_2$ is the submatrix that consists of the rows associated with $\{\mathbf{x}_n\}$, and $\mathbf{A} = \{a_{mn}\}$.

Note that $\mathbf{W}_2$ is a matrix related only to wavenumber $\mathbf{k}$. We propose to further decompose it as follows:

$$\mathbf{W_2} \approx \mathbf{C} \cdot \mathbf{B}, \tag{10}$$

where we determine $\mathbf{B}$ to be an $L \times N_x$ matrix, and the entry, $\mathbf{B}(\xi, \mathbf{k})$, has the form of $\cos(\sum_{j=1}^{3} \xi^j k_j \Delta x_j)$, in which ξ is a 3-D integer vector, $\xi = (\xi^1, \xi^2, \xi^3)$, k_j is the jth component of wavenumber $\mathbf{k}$, Δx_j is the space grid size in the jth direction, $j = 1, 2, 3$, and $\mathbf{C}$ is the

matrix product of $\mathbf{W}_2$ and the pseudo-inverse of $\mathbf{B}$. In practice, we apply a weighted-inversion to achieve the pseudo-inverse: putting a larger weight on the low-wavenumber part and a smaller weight on the high-wavenumber part to enhance the stability. Now we have a new decomposition for the mixed-domain matrix:

$$\mathbf{W} \approx \mathbf{G} \cdot \mathbf{B}, \tag{11}$$

where $\mathbf{G}$ is an $N_x \times L$ matrix,

$$\mathbf{G} = \mathbf{W}_1 \cdot \mathbf{A} \cdot \mathbf{C}, \tag{12}$$

and

$$\begin{aligned} p(\mathbf{x}, t+\Delta t) + p(\mathbf{x}, t-\Delta t) &= 2\int e^{-i\mathbf{x}\mathbf{k}} W(\mathbf{x}, \mathbf{k})\hat{p}(\mathbf{k}, t)d\mathbf{k} \\ &\approx 2\sum_{m=1}^{L} G(\mathbf{x}, m)\left(\int e^{-i\mathbf{x}\mathbf{k}} B(\xi_m, \mathbf{k})\hat{p}(\mathbf{k}, t)d\mathbf{k}\right) \\ &\approx \sum_{m=1}^{L} G(\mathbf{x}, m)\left(\int e^{-i\mathbf{x}\mathbf{k}} 2\cos\left(\sum_{j=1}^{3}\xi_m^j k_j \Delta x_j\right)\hat{p}(\mathbf{k}, t)d\mathbf{k}\right) \\ &\approx \sum_{m=1}^{L} G(\mathbf{x}, m)\left[\int e^{-i\mathbf{x}\cdot\mathbf{k}}(e^{i\sum_{j=1}^{3}\xi_m^j k_j \Delta x_j} + e^{-i\sum_{j=1}^{3}\xi_m^j k_j \Delta x_j})\hat{p}(\mathbf{k}, t)d\mathbf{k}\right]. \end{aligned} \tag{13}$$

According to the shift property of FFTs, we finally obtain an expression in the space-domain

$$p(\mathbf{x}, t+\Delta t)+p(\mathbf{x}, t-\Delta t)=\sum_{m=1}^{L} G(\mathbf{x}, m)[p(\mathbf{x}_L, t)+p(\mathbf{x}_R, t)], \tag{14}$$

where $\mathbf{x}_L = (x_1 - \xi_m^1\Delta x_1, x_2 - \xi_m^2\Delta x_2, x_3 - \xi_m^3\Delta x_3)$, and $\mathbf{x}_R = (x_1 + \xi_m^1\Delta x_1, x_2 + \xi_m^2\Delta x_2, x_3 + \xi_m^3\Delta x_3)$.

Eq. (14) indicates a procedure of finite differences for wave extrapolation: the integer vector, $\xi_\mathbf{m} = (\xi_m^1, \xi_m^2, \xi_m^3)$ provides the stencil information, and $G(\mathbf{x}, m)$ stores the corresponding coefficients. We call this method lowrank finite differences (LFD) because the finite-difference coefficients are derived from a lowrank approximation of the mixed-domain propagator matrix. We expect the derived LFD scheme to accurately propagate seismic-wave components within a wide range of wavenumbers, which has advantages over conventional finite differences that focus mainly on small wavenumbers. In comparison with the Fourier-domain approach, the cost is reduced to $O(L N_x)$, where L, as the row size of matrix $\mathbf{B}$, is related to the order of the scheme. L can be used to characterize the number of FD coefficients in the LFD scheme, shown in eq. (14). Take the 1-D 10th order LFD as an example, there are one center point, five left points ($\mathbf{x}_L$) and five right ones ($\mathbf{x}_R$). So $\xi_m^1 = 0, 1, 2, 3, 4, 5$ and $\xi_m = (\xi_m^1, 0, 0)$. Thanks to the symmetry of the scheme, coefficients of $\mathbf{x}_L$ and $\mathbf{x}_R$ are the same, as indicated by eq. (14). As a result, one only needs six coefficients: $L = 6$.

We use a 1-D example shown in Fig. 1 to demonstrate the accuracy of the proposed LFD method. The velocity linearly increases from 1000 to 2275 m s^{-1}. The rank is 3 ($M = N = 3$) for lowrank decomposition for this model with 1 ms time step. The propagator matrix is shown in Fig. 1(a). Figs 1(b)–(d) display the errors corresponding to different approximations. The error by the 10th-order LFD (Fig. 1c) appears significantly smaller than that of the 10th-order finite difference (Fig. 1d). Fig. 2 displays the middle column of the error matrix. Note that the error of the LFD is significantly closer to zero than that of the FD method.

To analyse the accuracy, we let

$$p(\mathbf{x}, t) = e^{i(\mathbf{k}\cdot\mathbf{x}-\omega t)}, \tag{15}$$

by using the plane wave theory. Inserting (15) into eq. (14) and also adopting the dispersion relation $\omega = |k|\, v$, defines the phase velocity of LFD (v_{LFD}) as follows:

$$v_{\mathrm{LFD}} = \frac{1}{|k|\Delta t}\arccos\left(\sum_{m=1}^{L} G(\mathbf{x}, m)\left(\cos\left(\xi_m^1 k_1 \Delta x_1\right) + \cos\left(\xi_m^2 k_2 \Delta x_2\right) + \cos\left(\xi_m^3 k_3 \Delta x_3\right)\right)\right). \tag{16}$$

For 1-D 10th order LFD, $L = 6$, $\xi_m = (\xi_m^1, 0, 0)$ and $\xi_m^1 = 0, 1, 2, 3, 4, 5$. With eq. (16), we can calculate phase-velocities (v_{LFD}) by 1-D 10th order LFD with different velocities ($v = 2500$, 3000, 3500, 4000), and we use the ratio $\delta = v_{\mathrm{LFD}}/v$ to describe the dispersion of FD methods. Fig. 3(a) displays 1-D dispersion curves by 1-D 10th order LFD, and Fig. 3(b) shows those by conventional FD method. Note that compared with the conventional FD method, LFD is accurate in a wider range of wavenumbers (up to 70 per cent of the Nyquist frequency).

2.3 TTI Lowrank Finite Differences

The LFD approach is not limited to the isotropic case. In the case of TTI media, the term $v(\mathbf{x})\,|\mathbf{k}|$ on the right-hand side of eq. (6), can be replaced with the acoustic approximation (Alkhalifah 1998, 2000; Fomel 2004),

$$f(\mathbf{v}, \hat{\mathbf{k}}, \eta) = \sqrt{\frac{1}{2}\left(v_1^2\hat{k}_1^2 + v_2^2\hat{k}_2^2\right) + \frac{1}{2}\sqrt{\left(v_1^2\hat{k}_1^2 + v_2^2\hat{k}_2^2\right)^2 - \frac{8\eta}{1+2\eta}v_1^2 v_2^2 \hat{k}_1^2\hat{k}_2^2}}, \tag{17}$$

where v_1 is the P-wave phase velocity in the symmetry plane, v_2 is the P-wave phase velocity in the direction normal to the symmetry plane, η is the anisotropic elastic parameter (Alkhalifah & Tsvankin 1995) related to Thomsen's elastic parameters ϵ and δ (Thomsen 1986) by

$$\frac{1+2\delta}{1+2\epsilon} = \frac{1}{1+2\eta}; \tag{18}$$

and $\hat{k}_1$ and $\hat{k}_2$ stand for the wavenumbers evaluated in a rotated coordinate system aligned with the symmetry axis:

$$\begin{aligned} \hat{k}_1 &= k_1\cos\theta + k_2\sin\theta \\ \hat{k}_2 &= -k_1\sin\theta + k_2\cos\theta, \end{aligned} \tag{19}$$

where θ is the tilt angle measured with respect to vertical.

Using these definitions, we develop a version of the LFD scheme for 2-D TTI media.

2.4 Lowrank Fourier Finite Differences

Song & Fomel (2011) proposed FFD approach to solve the two-way wave equation. The FFD operator is a chain operator that combines FFT and FD, analogous to the concept introduced previously for

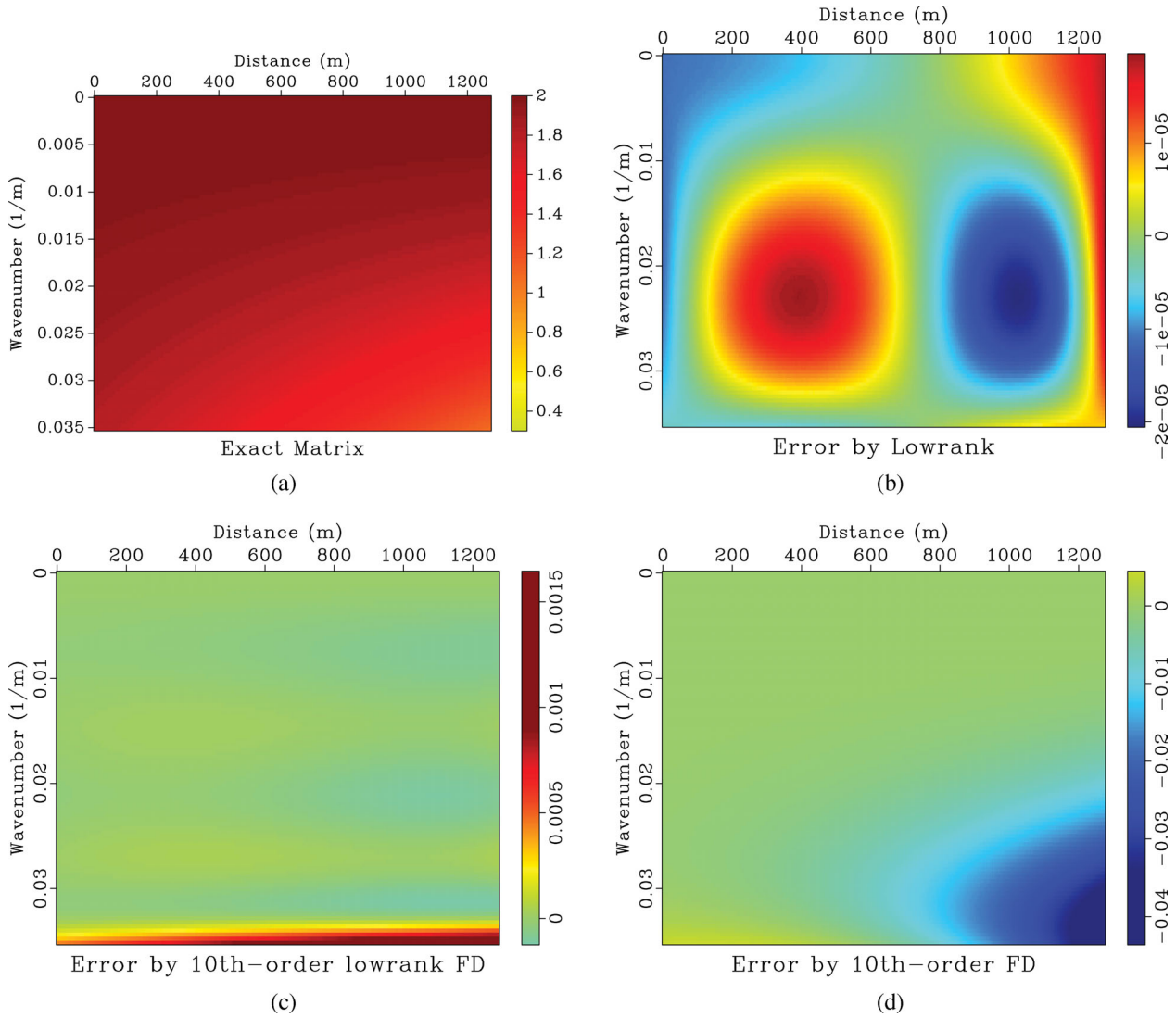

Figure 1. (a) Wavefield extrapolation matrix for 1-D linearly increasing velocity model. Error of wavefield extrapolation matrix by: (b) lowrank approximation, (c) the 10th-order lowrank FD, (d) the 10th-order FD.

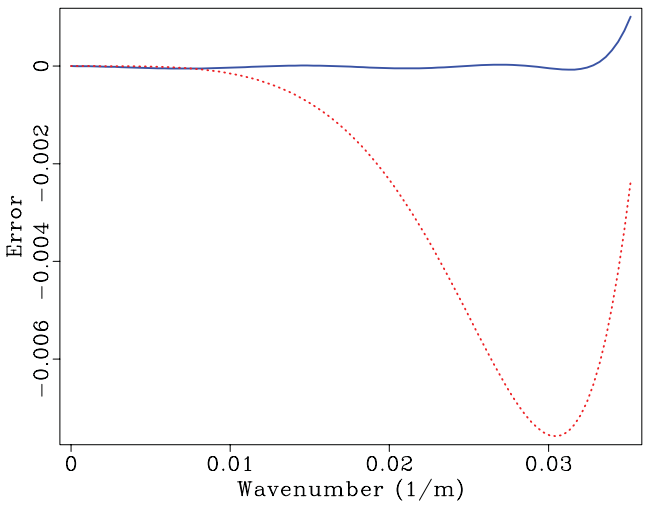

Figure 2. Middle column of the error matrix. Solid line: the 10th-order LFD. Dash line: the 10th-order FD.

one-way wave extrapolation by Ristow & Ruhl (1994). The FFD method adopts the pseudo-analytical solution of the acoustic wave equation, shown in eq. (5). It first extrapolates the current wavefield with some constant reference velocity and then applies FD to correct the wavefield according to local model parameter variations. In the TTI case, the FD scheme in FFD is typically a 4th-order operator, derived from Taylor's expansion around $k = 0$. However, it may exhibit some dispersion caused by the inaccuracy of the FD part. We propose to replace the original FD operator with lowrank FD to increase the accuracy of FFD in isotropic and anisotropic media. We call the new operator lowrank Fourier Finite Differences (LFFD).

3 NUMERICAL EXAMPLES

Our first example is wave extrapolation in a 2-D, smoothly variable velocity model. The velocity ranges between 500 and 1300 m s^{-1}, and is formulated as

$$v(x,z) = 500 + 1.2 \times 10^{-4}(x-800)^2 + 10^{-4}(z-500)^2; \quad (20)$$

$0 \le x \le 2560, 0 \le z \le 2560$. A Ricker-wavelet source with a 20 Hz dominant frequency (f_d) is located at the center of the

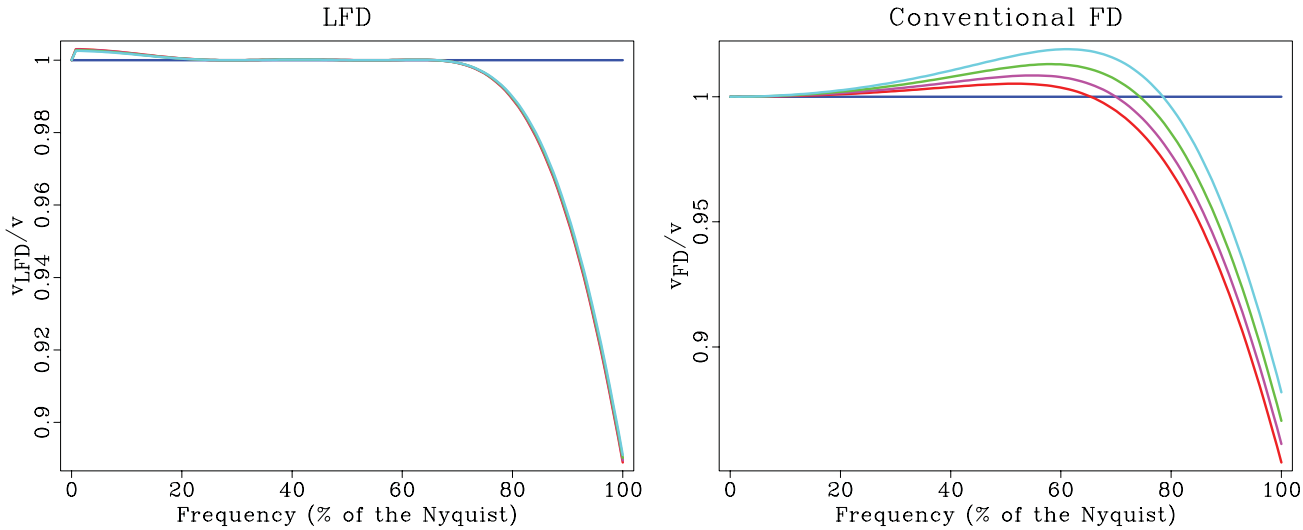

Figure 3. Plot of 1-D dispersion curves for different velocities, $v = 2500$ (red), 3000 (pink), 3500 (green), 4000 (blue) m s^{-1}, $\Delta t = 1$ ms, $\Delta x = 10$ m by: (a) the 10th-order LFD, (b) the 10th-order conventional FD.

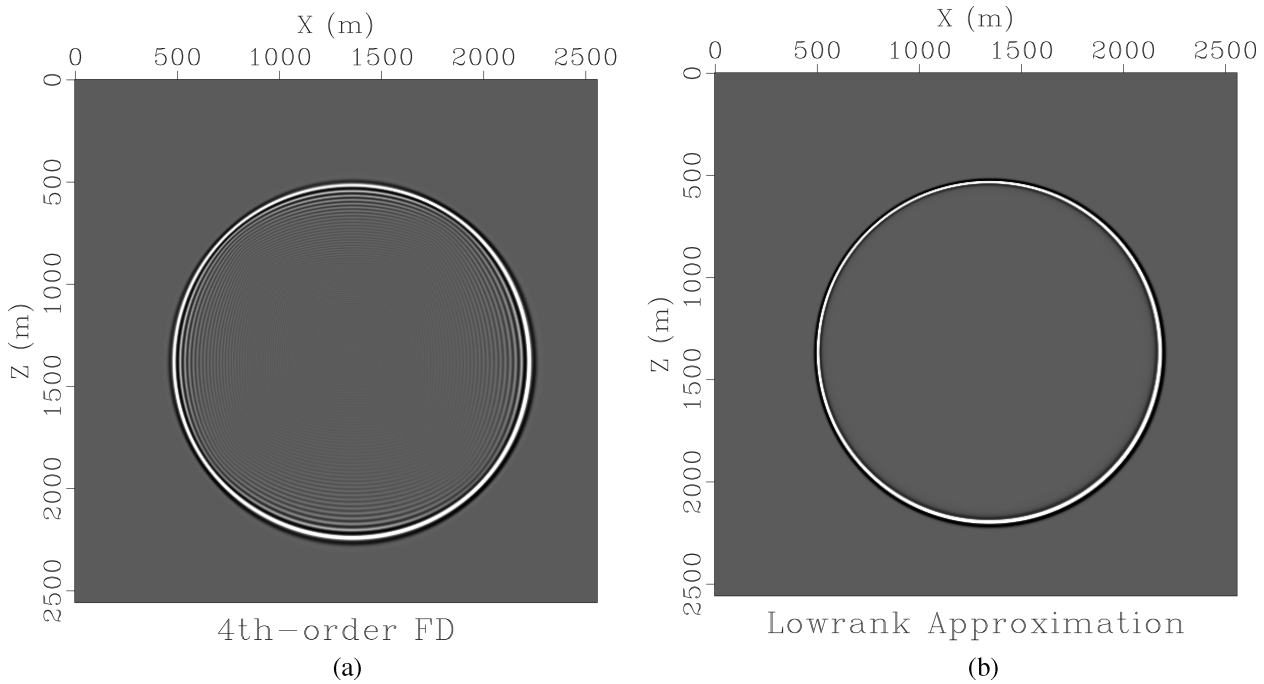

Figure 4. Wavefield snapshot in a variable velocity field by: (a) conventional 4th-order FD method, (b) Lowrank method.

model. The maximum frequency (f_{max}) is around 60 Hz. The amplitude corresponding to f_{max} is about 10^{-5} of that of f_d. For numerical simulations based on this model, we use the same grid size: $\Delta x = 5$ m and $\Delta t = 2$ ms. We use $\alpha = v_{max}\,\Delta t/\Delta x$ to specify the stability condition and $\beta = v_{min}/(f_{max}\Delta x)$ as the dispersion factor, where v_{max} and v_{min} are the maximum and minimum velocities of the model. The dispersion factor β indicates the number of sampling points for the minimum wavelength. For simulations with the above parameters, $\alpha \approx 0.52$ and $\beta \approx 1.67$.

It is easy to observe obvious numerical dispersions on the snapshot computed by the 4th-order FD method (Fig. 4a). The lowrank FD method with the same order exhibits higher accuracy and fewer dispersion artefacts (Fig. 5a). The approximation rank decomposition in this case is $N = 3$ $M = 4$, with the expected error of less than 10^{-4}. Fig. 5(b) displays the snapshot by the 10th-order LFD method with a larger time step: $\Delta t = 2.5$ ms, $\alpha \approx 0.65$. Note that the result is still accurate. However, the regular FD method becomes unstable in this case. For comparison, Fig. 4(b) displays the snapshot by the lowrank method with the same time step. The approximation rank decomposition in this case is $N = M = 3$, with the expected error of less than 10^{-4}. Thanks to the spectral nature of the algorithm, the result appears accurate and free of dispersion artefacts.

Next, we test the lowrank FD method in a complex velocity model. Fig. 6 shows a part of the BP velocity model (Billette & Brandsberg-Dahl 2004), which is a complicated model containing a salt body and sharp velocity contrasts on the flanks of the salt body.

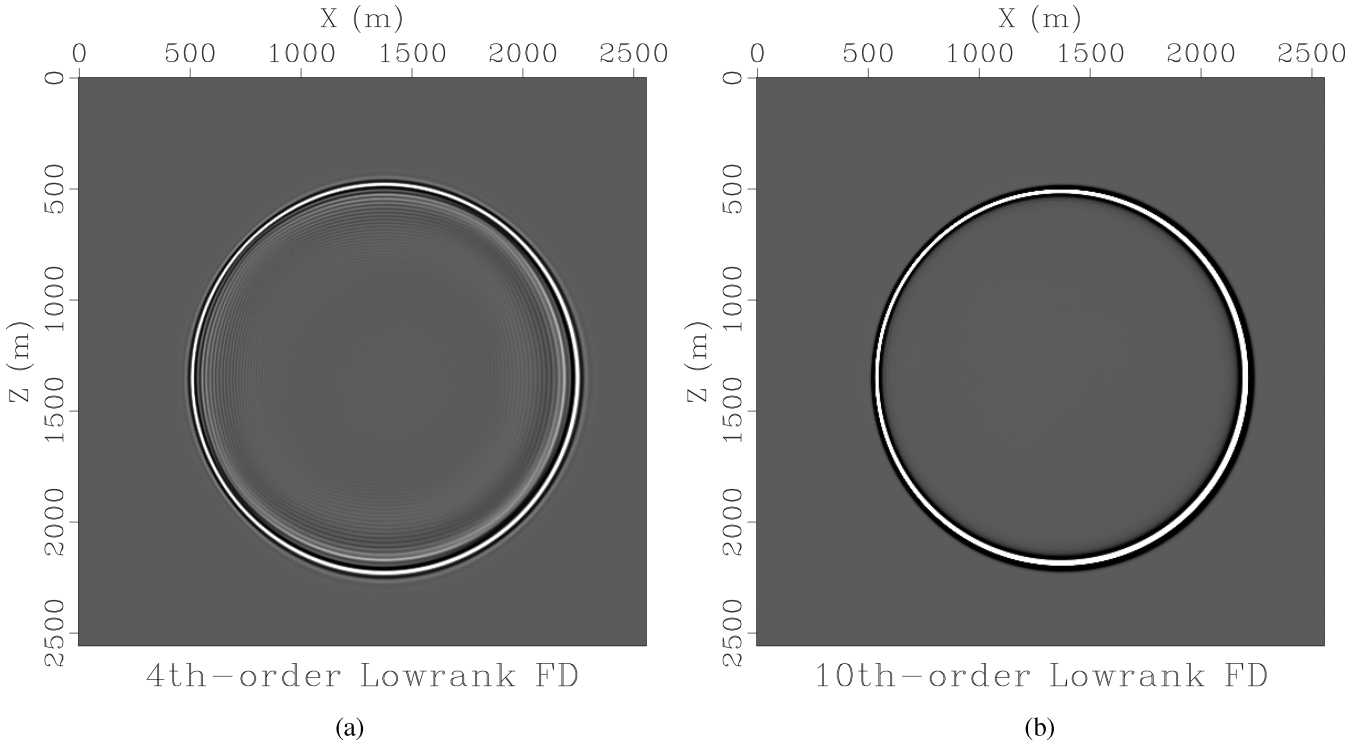

Figure 5. Wavefield snapshot in a variable velocity field by: (a) the 4th-order lowrank FD method, (b) the 10th-order lowrank FD method. Note that the time step is 2.5 ms and the LFD result is still accurate. However, the FD method is unstable in this case.

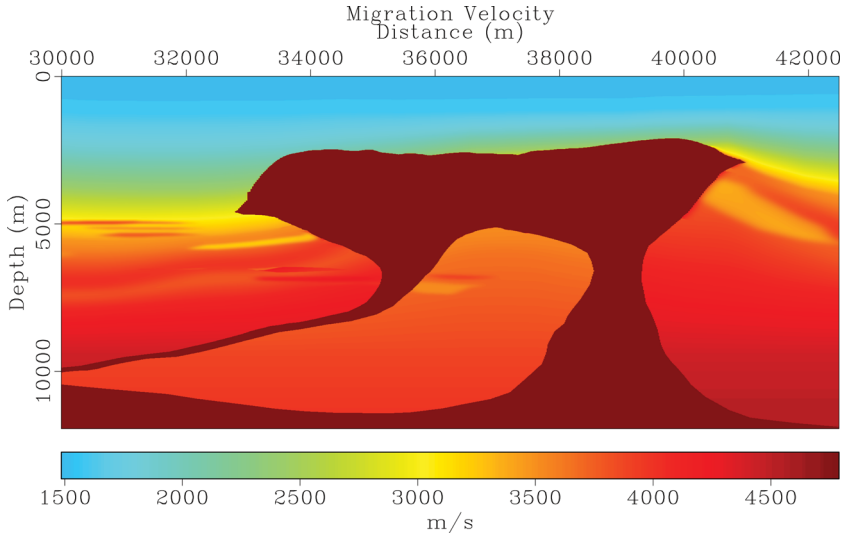

Figure 6. Portion of BP 2004 synthetic velocity model.

We use a Ricker-wavelet at a point source. The dominant frequency is 17 Hz ($f_{\max} \approx 54$). The horizontal grid size Δx is 12.5 m, the vertical grid size Δz is 12.5 m, and the time step is 1.5 ms. Thus $\alpha \approx 0.57$ and $\beta \approx 2.2$. The approximation rank decomposition in this case is $N = 4\, M = 5$, with the expected error of less than 10^{-4}. In this case, we adopt a disk-shaped compact scheme (8th-order) for LFD with a four-point radius ($|\xi| \leq 4, L = 25$). Fig. 7 displays a wavefield snapshot in the above velocity model. The snapshot is almost free of dispersions. This experiment confirms that the lowrank FD method is able to handle sharp velocity variations.

Our next example is wave propagation in a TTI model with a tilt of 45° and smooth velocity variation (v_x: 800–1225.41 m s^{-1}, v_z: 700–883.6 m s^{-1}). Fig. 8(a) shows wavefield snapshots at different time steps by a 16th-order LFD operator in the TTI model. The space grid size is 5 m and the time step size is 2 ms. So $\alpha \approx 0.49$ and $\beta \approx 2.3$. The approximation rank decomposition in this case is $N = 6\, M = 6$, with the expected error of less than 10^{-4}. For TTI model, we adopt a high-order (16th order) LFD operator to reduce dispersions. The scheme is compact and shaped as a disk with a radius of eight points ($L = 99$).

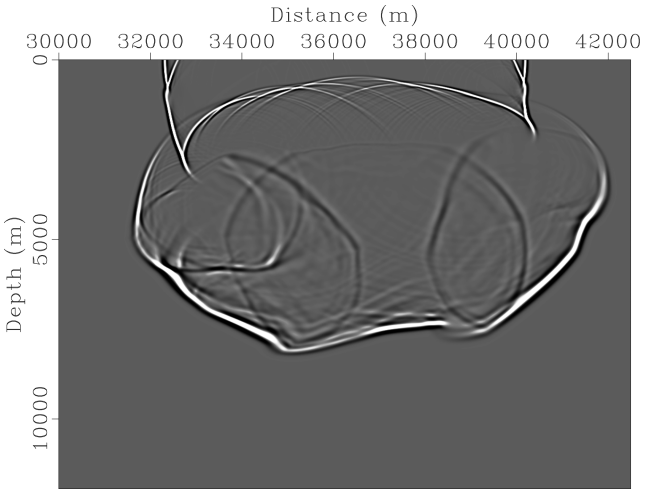

Figure 7. Wavefield snapshot by the 8th-order lowrank FD (compact scheme) in the BP Model shown in Fig. 6.

Song & Fomel (2011) showed an application of FFD method for TTI media. However, the example wavefield snapshot by FFD method still had some dispersion caused by the fact that the FD scheme in the FFD operator is derived from Taylor's expansion around zero wavenumber. It was apparent that 4th-order FD scheme is not accurate enough for TTI case and requires denser sampling per wavelength ($\beta \approx 4.6$). We first apply lowrank approximation to the mixed-domain velocity correction term in FFD. The rank is $N = 9\,M = 9$, with the expected error of less than 10^{-6}. Then we propose to replace that 4th-order FD operator with an 8th-order LFD compact scheme. The scheme has the shape of a disk with a radius of 4 points ($L = 25$), the same as the one for LFD in the above BP model. Fig. 8(b) shows wavefield snapshots by the proposed LFFD operator. The time step size is 1.5 ms ($\alpha \approx 0.37$). Note that the wavefront is clean and almost free of dispersion with $\beta \approx 2.3$. Because we use the exact dispersion relation, eq. (17) for TTI computation, there is no coupling of *q-SV* wave and *q-P* wave (Grechka *et al.* 2004; Duveneck *et al.* 2008; Zhang *et al.* 2009) in our snapshots by either LFD or LFFD methods.

Next we test the LFD and LFFD methods in a complex TTI model. Figs 9(a)–(d) shows parameters for part of the BP 2D TTI model (Shah 2007). The dominant frequency is 15 Hz ($f_{\max} \approx 50$). The space grid size is 12.5 m and the time step is 1 ms. Thus $\alpha \approx 0.42$ and $\beta \approx 2.4$. The approximation rank decomposition for LFD method is $N = 22$, $M = 22$, with the expected error of less than 10^{-6}. For FFD, $N = 24\,M = 30$, with the expected error of less than 10^{-6}. Both methods are able to simulate an accurate *qP*-wave field in this model as shown in Figs 10(a) and (b).

It is difficult to provide analytical stability analysis for LFD and LFFD operators. In our experience, the values of α are around 0.5 for 2-D LFD and LFD methods appear to allow for a larger time step size than that of the LFFD method. In TTI case, the conventional FD method for acoustic TTI has known issues of instability caused by shear wave numerical artefacts or sharp changes in the symmetry-axis tilting (Grechka *et al.* 2004; Duveneck *et al.* 2008; Zhang *et al.* 2009). Conventional methods may place limits on anisotropic parameters, smooth parameter models or include a finite shear wave velocity to alleviate the instability problem(Zhang & Zhang 2008; Fletcher *et al.* 2009; Yoon *et al.* 2010). Both LFD and LFFD methods are free of shear wave artefacts. They require no particular

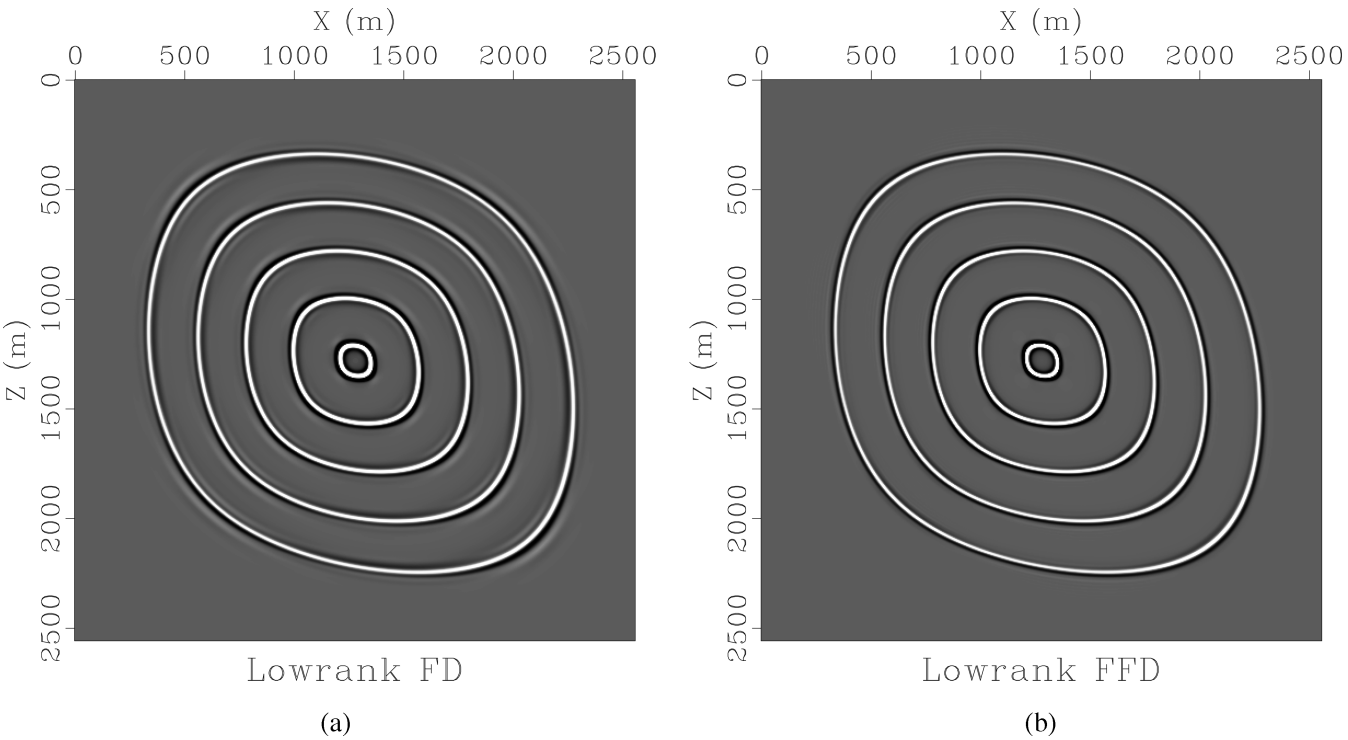

Figure 8. Wavefield snapshots in a TTI medium with a tilt of 45° by: (a) Lowrank FD method; (b) Lowrank FFD method.$v_x(x, z) = 800 + 10^{-4}(x - 1000)^2 + 10^{-4}(z - 1200)^2$; $v_z(x, z) = 700 + 10^{-4}(z - 1200)^2$; $\eta = 0.3$; $\theta = 45^\circ$.

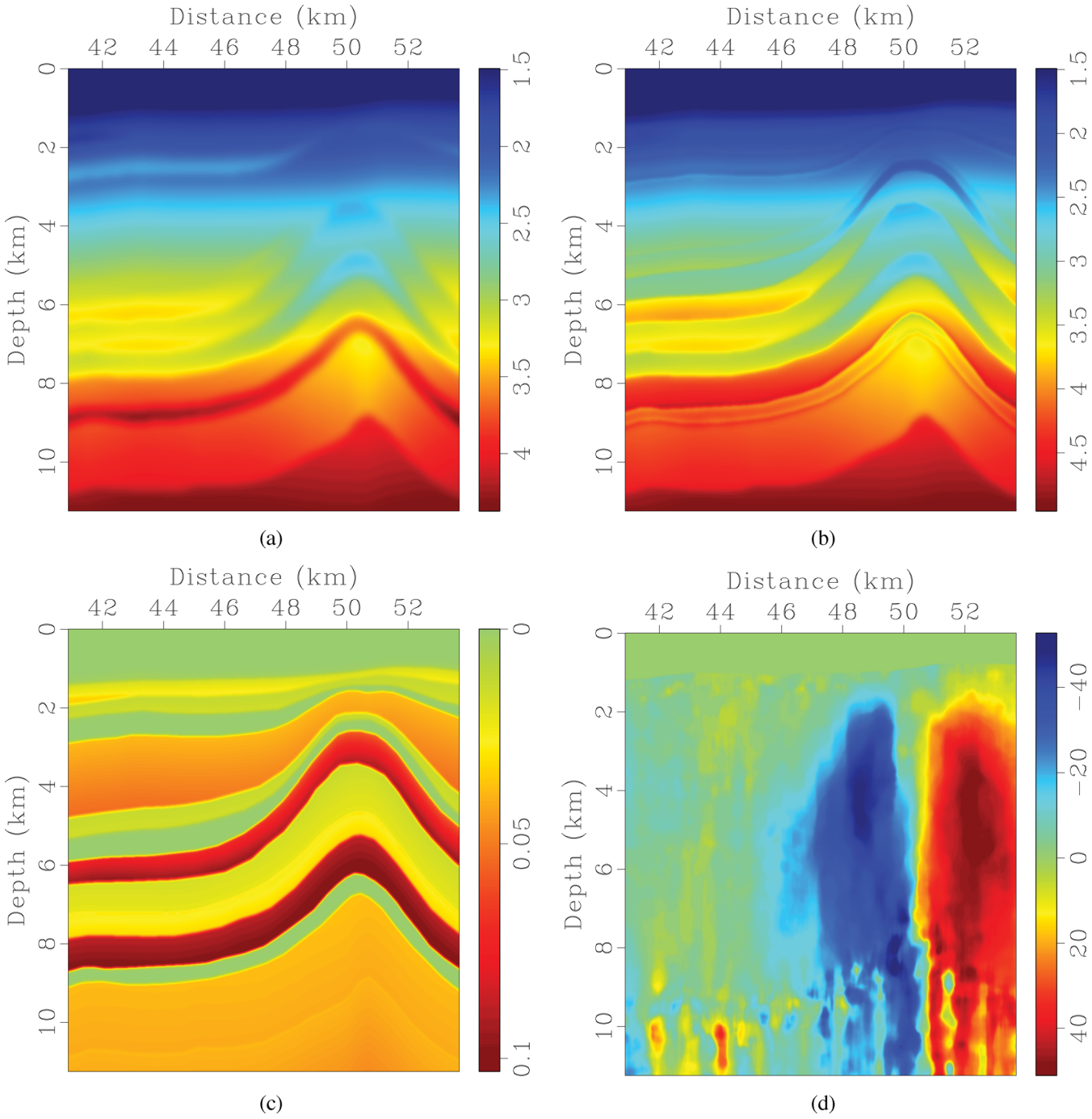

Figure 9. Partial region of the 2D BP TTI model. a: v_z. b: v_x. c: η. d:θ.

bounds for anisotropic parameters and can also handle sharp tilt changes.

4 CONCLUSIONS

Explicit finite difference (FD) methods are the most popular and straightforward methods for seismic modelling and seismic imaging, particularly for reverse-time migration. Traditionally the coefficients of FD schemes are derived from a Taylor series expansion around the zero wavenumber. We present a novel FD scheme: LFD, which is based on the lowrank approximation of the mixed-domain space-wavenumber propagator. LFD uses compact FD schemes, which are more suitable for parallelization on multi-core computers than spectral methods that require FFT operations. This technique promises higher accuracy and better stability than those of the conventional, explicit FD method. We also propose to replace the 4th-order FD operator based on Taylor's expansion in Fourier Finite Differences (FFD) with an 8th-order LFD operator to reduce dispersion, particularly in the TTI case. Results from synthetic experiments illustrate the stability of the proposed methods in complicated velocity models. In TTI media, there is no coupling of *qP*-waves and *qSv*-waves by either method. Both methods can be incorporated in seismic imaging by reverse-time migration to enhance its accuracy and stability.

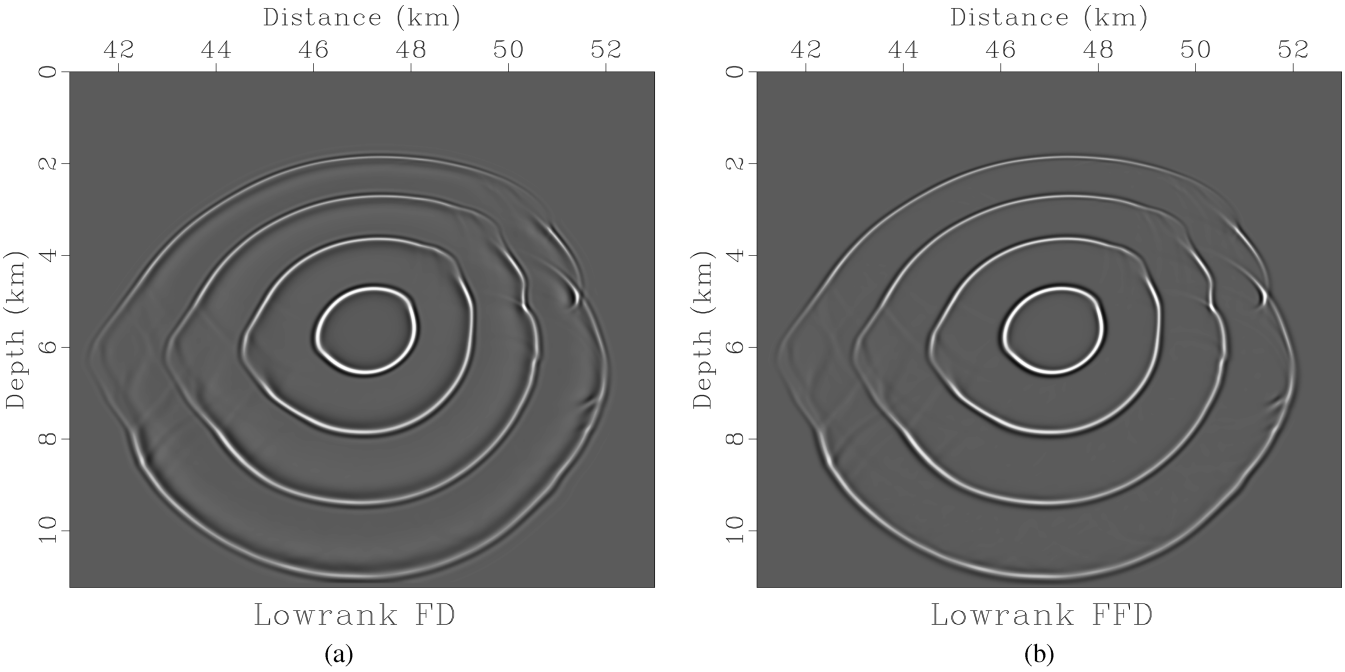

Figure 10. Scalar wavefield snapshots by LFD and LFFD methods in the 2-D BP TTI model.

REFERENCES

Alkhalifah, T., 1998. Acoustic approximations for processing in transversely isotropic media, *Geophysics,* **63,** 623–631.

Alkhalifah, T., 2000. An acoustic wave equation for anisotropic media, *Geophysics,* **65,** 1239–1250.

Alkhalifah, T. & Tsvankin, I., 1995. Velocity analysis for transversely isotropic media, *Geophysics,* **60,** 1550–1566.

Billette, F.J. & Brandsberg-Dahl, S., 2004. The 2004 BP velocity benchmark, in *Proceedings of the 67th Annual EAGE Meeting, EAGE, Expanded Abstracts,* p. B305.

Cheng, J. & Kang, W., 2012. Propagating pure wave modes in 3D general anisotropic media, Part I: P-wave propagator, in *Proceedings of the 82nd Annual International Meeting,* Soc. of Expl. Geophys.

Chu, C. & Stoffa, P.L., 2011. Application of normalized pseudo-Laplacian to elastic wave modeling on staggered grids, *Geophysics,* **76**(5), T113–T121.

Dablain, M.A., 1986. The application of high-order differencing to the scalar wave equation, *Geophysics,* **51**(1), 54–66.

Duveneck, E., Milcik, P., Bakker, P.M. & Perkins, C., 2008. Acoustic VTI wave equations and their application for anisotropic reverse-time migration, in *78th Ann. Internat. Mtg.,* pp. 2186–2190, Soc. of Expl. Geophys.

Engquist, B. & Ying, L., 2009. A fast directional algorithm for high frequency acoustic scattering in two dimensions, *Commun. Math. Sci.,* **7**(2), 327–345.

Etgen, J., 1989. Accurate wave equation modeling, *SEP-60,* pp. 131–147.

Etgen, J. & Brandsberg-Dahl, S., 2009. The pseudo-analytical method: application of pseudo-Laplacians to acoustic and acoustic anisotropic wave propagation, in *79nd Annual International Meeting, SEG, Expanded Abstracts,* pp. 2552–2556.

Etgen, J., Gray, S.H. & Zhang, Y., 2009. An overview of depth imaging in exploration geophysics, *Geophysics,* **74**(6), WCA5–WCA17.

Finkelstein, B. & Kastner, R., 2007. Finite difference time domain dispersion reduction schemes, *J. Comput. Phys.,* **221,** 422–438.

Fletcher, R.P., Du, X. & Fowler, P.J., 2009. Reverse time migration in tilted transversely isotropic (TTI) media, *Geophysics,* **74**(6), WCA179–WCA187.

Fomel, S., 2004. On anelliptic approximations for qP velocities in VTI media, *Geophys. Prospect.,* **52,** 247–259.

Fomel, S., Ying, L. & Song, X., 2010. Seismic wave extrapolation using a lowrank symbol approximation, in *80th Annual International Meeting,* pp. 3092–3096, Society of Exploration Geophysicists.

Fomel, S., Ying, L. & Song, X., 2012. Seismic wave extrapolation using lowrank symbol approximation, *Geophys. Prospect,* doi:10.1111/j.1365-2478.2012.01064.x.

Fornberg, B., 2002. *A Practical Guide to Pseudo-spectral Methods (Cambridge Monographs on Applied and Computational Mathematics),* Cambridge University Press.

Fowler, P.J. & Lapilli, C., 2012. Generalized pseudospectral methods for modeling and reverse-time migration in orthorhombic media, in *1 Proceedings of the 74th Annual EAGE Meeting, EAGE, Expanded Abstracts,* p. AO22.

Gazdag, J., 1981. Modeling of the acoustic wave equation with transform methods, *Geophysics,* **46**(6), 854–859.

Geller, R.J. & Takeuchi, N., 1995. A new method for computing highly accurate DSM synthetic seismograms, *Geophys. J. Int.,* **123,** 449–470.

Geller, R.J. & Takeuchi, N., 1998. Optimally accurate second-order time domain finite difference scheme for the elastic equation of motion: 1-D case, *Geophys. J. Int.,* **135,** 48–62.

Grechka, V., Zhang, L. & Rector, J.W., 2004. Shear waves in acoustic anisotropic media, *Geophysics,* **69,** 576–582.

Holberg, O., 1987. Computational aspect of the choice of operator and sampling interval for numerical differentiation in large scale simulation of wave phenomena, *Geophys. Prospect.,* **35,** 629–655.

Holberg, O., 1988. Towards optimum one-way wave propagation, *Geophysics,* **36,** 99–114.

Kindelan, M., Kamel, A. & Sguazzero, P., 1990. On the construction and efficiency of staggered numerical differentiators for the wave equation, *Geophysics,* **55**(1), 107–110.

Liu, Y. & Sen, M.K., 2009. A new time-space domain high-order finite-difference method for the acoustic wave equation, *J. Comput. Phys.,* **228,** 8779–8806.

Liu, Y. & Sen, M.K., 2011. Finite-difference modeling with adaptive variable-length spatial operators, *Geophysics,* **76,** T79–T89.

Mousa, W.A., van der Baan, M., Boussakta, S. & McLernon, D.C., 2009. Designing stable extrapolators for explicit depth extrapolation of 2D and 3D wavefields using projections onto convex sets, *Geophysics,* **74,** S33–S45.

Ristow, D. & Ruhl, T., 1994. Fourier finite-difference migration, *Geophysics,* **59,** 1882–1893.

Shah, H., 2007. The 2007 BP anisotropic velocity-analysis benchmark, in *Proceedings of the 70th Annual EAGE Meeting, EAGE,* Workshop.

Song, X. & Fomel, S., 2011. Fourier finite-difference wave propagation, *Geophysics,* **76**(5), T123–T129.

Song, X., Nihei, K. & Stefani, J., 2012. Seismic modeling in acoustic variable-density media by fourier finite differences, in *Proceedings of the 82th Annual International Meeting*.

Soubaras, R., 1996. Explicit 3-D migration using equiripple polynomial expansion and laplacian synthesis, *Geophysics,* **61,** 1386–1393.

Soubaras, R. & Zhang, Y., 2008. Two-step explicit marching method for reverse time migration, in *Proceedings of the 78th Ann. Internat. Mtg.,* pp. 2272–2276, Soc. Expl. Geophys.

Tabei, M., Mast, T.D. & Waag, R.C., 2002. A k-space method for coupled first-order acoustic propagation equations, *J. acoust. Soc. Am.,* **111**(1), 53–63.

Takeuchi, N. & Geller, R.J., 2000. Optimally accurate second order time-domain finite difference scheme for computing synthetic seismograms in 2-D and 3-D media, *Phys. Earth planet. Int.,* **119,** 99–131.

Thomsen, L., 1986. Weak elastic anisotropy, *Geophysics,* **51,** 1954–1966.

Wu, W., Lines, L.R. & Lu, H., 1996. Analysis of high-order, finite-difference schemes in 3-D reverse-time migration, *Geophysics,* **61,** 845–856.

Yoon, K., Suh, S., Ji, J., Cai, J. & Wang, B., 2010. Stability and speedup issues in TTI RTM implementation, in *Proceedings of the 80th Ann. Internat. Mtg.,* pp. 3221–3225, Soc. Expl. Geophys.

Zhan, G., Pestana, R.C. & Stoffa, P.L., 2012. Decoupled equations for reverse time migration in tilted transversely isotropic media, *Geophysics,* **77,** T37–T45.

Zhang, H. & Zhang, Y., 2008. Reverse time migration in 3D heterogeneous TTI media, in *Proceedings of the 78th Annual International Meeting,* pp. 2196–2200, Soc. of Expl. Geophys.

Zhang, H., Zhang, G. & Zhang, Y., 2009. Removing s-wave noise in TTI reverse time migration, in *Proceedings of the 79th Annual International Meeting,* pp. 2849–2853, Soc. of Expl. Geophys.